Original Research Article

Modelling Salt Rejection in Nanofiltration and Reverse Osmosis Membranes Using the Spiegler-Kedem Model Enhanced by a Bio-Inspired Metaheuristic Algorithms: Particle Swarm Optimization and Grey Wolf Optimization

Bouchra Abbi[1], Azzeddin Touazit[1], Oussama Gliti[1], Mohammed Igouzal*[1], Maxime Pontie[2], Abdérafi Charki[3], Thierry Lemenand[3]

[1]Laboratory of Electronic Systems Information Processing Mechanics and Energy, Ibn Tofail University, Kenitra, Morocco
e-mail: bouchra.abbi@uit.ac.ma, azzeddin.touazit@uit.ac.ma, Oussama.gliti@uit.ac.ma, mohammed.igouzal@uit.ac.ma

[2]Group of Analysis and Processes, Faculty of sciences, Angers Univesity, 2 Bd; Lavoisier, 49045 Angers cedex01, France
e-mail: maxime.pontie@univ-angers.fr

[3]LARIS, University of Angers, France
e-mail: abderafi.charki@univ-angers.fr, thierry.lemenand@univ-angers.fr

ABSTRACT

Pressure-driven membrane processes, such as reverse osmosis and nanofiltration, represent credible processes for salinity reduction in ground, surface, and seawater, as well as in mining and urban wastewater. The separation characteristics and productivity of these processes depend on several factors, including molecular weight cut-off and operating conditions (applied pressure, recovery rate..). This study aims to model salt rejection performance of water in Tan Tan City (Morocco) using nanofiltration membranes (NF90, NF200, NE90) and reverse osmosis membranes (BW30LE), under various operational conditions, used the Spiegler-Kedem model. Both the Particle Swarm Optimization and Grey Wolf Optimization algorithms were applied to optimize the model parameters to fit experimental data. The results showed excellent agreement between experimental rejection rates and model-predicted rejection rates for both algorithms. Additionally, Grey Wolf Optimization model gave slightly better results compared to Particle Swarm Optimization. The combined use of a well-established theoretical framework and efficient optimization algorithms provides a significant step forward in the quest for reliable and sustainable water resources.

KEYWORDS

INTRODUCTION

The increasing demand for freshwater resources, coupled with the decline of natural water resources, has led to the rapid development of desalination technologies [1], [2]. Pressure-driven membrane processes, such as nanofiltration (NF) and reverse osmosis (RO), have become some of the most advanced and effective techniques for separating salts and other

compounds from water sources [3]. Membrane usage is expanding rapidly across various fields, with desalination of brackish and saline water being a prominent application [4], [5]. Pressure-driven membranes are particularly significant among desalination techniques. Classical reverse osmosis is widely recognized as a standard method for desalination [2]. However, membrane technology can be a competitive separation technique due to its superior performance and cost efficiency compared to traditional filtration processes [6], [7].

Many software such as ROSA, Winflow, and IMS have been developed and implemented in designing RO systems [8]. These software packages calculate and give warnings about design errors, such as feed pressure or recovery ratio exceeding membrane limits. The ROSA software, in particular, was validated through an extensive case study [8], filling a gap in the literature by simplifying the parameter classification and offering a clear, verified approach to system design.

The majority of modelling works in membrane studies have utilized models based in the extended Nernst-Planck equation [9]. These models are developed based on a comprehensive understanding of the physical mechanisms underlying membrane processes [10]. They exhibit mathematical complexity and entail considerable computational resources, demanding a thorough comprehension of the filtration process and membrane characteristics [9]. Consequently, it appears necessary to explore alternative methods for predicting process performance, leveraging existing process data and extrapolating it to inaccessible data. The Spiegler-Kedem model emerges as a viable option for modelling intricate and nonlinear membrane systems [11].

The Spiegler-Kedem model has been used in many previous studies on modelling salt rejection in membranes to understand transport phenomena in these membranes [12], [13]. For instance, Pontié et al. (2008) [11] combined mass transfer modelling with physicochemical characterization to highlight the relevance of the Spiegler-Kedem model for NF and RO membranes. Spiegler and Kedem (1966) [14] established the model's thermodynamic foundations, while Bowen and Mukhtar (1996) [15] validated its effectiveness in characterizing membrane selectivity. These studies showed that the Spiegler-Kedem model views membranes as a black box and characterizes them using two parameters: salt permeability (Ps) and reflection coefficient (σ) [11]. While the Spiegler-Kedem model can provide reasonable predictions of salt rejection for a variety of membrane processes [13]. However, this model often requires extensive experimental data and is limited by its complexity and computational demands [10].

To address these limitations and enhance the precision of model fitting, recent studies have explored the use of Bio-inspired metaheuristic algorithms as effective tools for solving complex optimization problems in membrane modelling processes more efficiently [16], [17], [18]. Many experts have studied salt rejection using these algorithms [19], [20], [21], particularly those based on swarm intelligence, such as Particle Swarm Optimization (PSO) and Grey Wolf Optimization (GWO). For instance, Mahadeva et al. (2021) [17] used PSO and neural networks for reverse osmosis simulation, improving prediction accuracy, while Maftouh et al. (2023) [20] and Rabah et al. (2024) [21] explored solar desalination and sustainability frameworks. Rinawati et al. (2024) [22] focused on contaminant removal optimization. PSO is inspired by the social behaviour of birds flocking or fish schooling [23], while GWO mimics the leadership hierarchy and hunting mechanism of grey wolves [23].

Early studies on water treatment using desalination technologies in Tan Tan City (Morocco) have been carried out since 2001 [24]. Tan Tan was selected as a case study due to its increasing reliance on desalination to meet freshwater demands in an arid environment. All these studies were based on field measurements of and did not examine the evolution influence of salt rejection toward under various operational conditions. Tahri (2001) [24] investigated freshwater supply prospects from non-conventional water sources for the region, including desalination, while Pontié et al. (2006) [25] focused on the application of nanofiltration for

Abbi, B., Touazit, A., *et al.*
Modelling Salt Rejection in Nanofiltration and Reverse...

Year 2025
Volume 13, Issue 3, 1130565

large-scale pilot plants, highlighting its potential for improving water quality. These studies, however, did not explore the optimization of membrane processes under varying conditions. In addition, they recommended the applied of theoretical model for optimizing parameters in membrane process [26], [27]. In a management context, rapid estimation of salt rejection percentage as a function of permeate flux in given membranes is searched by managers [28]. The Spiegler-Kedem model, coupled with bio-inspired metaheuristic algorithms for optimization can constitute the appropriate tools to use because they are easy to apply, and more adapted to management contexts. Also, it is methodologically correct to start with the simplest description of the phenomena under study and to evaluate the limits of this approximation before investigating more complex models [29], [30].

This study aims to model salt rejection in NF and RO membranes using an approach that integrates the Spiegler-Kedem model with the GWO and PSO algorithms (referred to as the SKM-PSO and SKM-GWO approaches). The study examines three different Nanofiltration membranes (NF200, NE90, NF90) and one Reverse osmosis membrane (BW30LE) under varying operational conditions, including applied pressure and recovery rate. The experimental tests were conducted using feed water from Tan Tan City, Morocco, to evaluate membrane performance under real conditions. The GWO and PSO algorithms were used to optimize model parameters, specifically reflection coefficient (σ) and salt permeability (Ps), to fit experimental data.

The utilization of the Spiegler-Kedem model provides a robust theoretical framework for simulating salt rejection performance. This model allows to delve into the complex interplay of membrane characteristics and operational parameters, offering valuable insights into the intricacies of salt rejection processes [5]. To improve the accuracy and reliability of the modelling, the optimization process of the PSO and GWO algorithms was exploited. These algorithms efficiently tune the model parameters to match the experimental data, thus bridging the gap between theoretical predictions and real-world observations [18].

The integration of the PSO and GWO algorithms with a well-established thermodynamic model represents a novel and powerful approach (SKM-PSO and SKM-GWO) to improving the precision of salt rejection model predictions for NF and RO membranes. This integration reduces the need for extensive experimental data, thus making the modelling process more practical and manageable. Furthermore, it provides valuable information for the design and operational stages of desalination plants. The model has been used to explain real-world scenarios, underpinning practical applications in regions susceptible to salinity and water treatment processes. Consequently, this approach offers valuable insights that could contribute significantly to the sustainable management of water resources.

The current study validates the recommendations from previous research regarding the application of theoretical models for optimizing parameters in membrane processes. Both SKM-PSO and SKM-GWO models have demonstrated high effectiveness in optimizing parameters for membrane modelling. Additionally, a comparative analysis of these algorithms was performed to determine the most efficient optimization technique. The results indicated that the SKM-GWO model produced slightly better outcomes compared to the SKM-PSO model.

METHODS

In the study of membrane processes, accurate modelling is essential for predicting performance and optimizing operational parameters. This section presents a comprehensive approach to modelling membrane behaviour using the Spiegler-Kedem model. To enhance the model's accuracy and efficiency, advanced bio-inspired metaheuristic algorithms was employed, specifically PSO and GWO. These methods effectively optimize complex, nonlinear problems effectively, providing robust solutions for improving membrane performance.

Abbi, B., Touazit, A., *et al.*
Modelling Salt Rejection in Nanofiltration and Reverse...

Year 2025
Volume 13, Issue 3, 1130565

Spiegler Kedem model

Membrane performance is evaluated based on membrane rejection, R (%), and permeate flux, Jp (m.s^{-1}). When dealing with dilute aqueous mixtures containing water and a solute, the membrane's selectivity towards the mixture is commonly expressed using the observed solute rejection coefficient [31], [32]. This coefficient quantifies the membrane's effectiveness in separating the solute from the feed solution and is defined as a percentage as follows:

$$R = 100 \times \left(1 - \frac{C_p}{C_f} \right) \tag{1}$$

Where, Cf (mg.L^{-1}) is the solute concentration at the feed membrane interface, Cp (mg.l^{-1}) is the permeate solute concentration [33].

The permeate flux is determined using the following equation [34]:

$$J_P = \frac{Q_P}{S} \tag{2}$$

Where Q_p is the volumetric permeate flux (m^3.s^{-1}), and S represents the membrane's active area (m^2).

The Spiegler-Kedem model, based on irreversible thermodynamics models, provides a straightforward framework for describing solute transport in both RO and NF processes [35]. In this model, the membrane is considered as a black box, where interactions between solute and solvent species are taken into account. Starting with the assumption that water flux (J_v) and solute flux (J_s) are propelled by forces F_v and F_s, respectively, stemming from chemical potential gradients across the membrane, the model derives equations relating these fluxes to membrane coefficients [14]. By integrating these principles, the equations provided by Kedem and Katchalsky make it possible to establish a relationship between water and solute fluxes as well as membrane coefficients [34]. These coefficients include hydraulic permeability (L_p), solute permeability (P_s), and reflection coefficient (σ) [36]:

$$J_v = L_{ii}F_v + L_{ij}F_s \tag{3}$$

$$J_s = L_{ji}F_v + L_{jj}F_s \tag{4}$$

Where L_{ii}, L_{jj}, L_{ij} and L_{ji} are phenomenological coefficients.

The chemical potential gradient arises from either a concentration or pressure gradient. Consequently, the ultimate operational equations of the nonlinear Spiegler-Kedem model are [37]:

$$J_v = L_P (\Delta P - \sigma \Delta \Pi) \tag{5}$$

$$J_S = P_S (C_m - C_P) + (1 - \sigma) J_v C_m \tag{6}$$

ΔP represents the transmembrane pressure, while $\Delta \Pi$ indicates the difference in osmotic pressure across the membrane (bar). C_m (mg. L^{-1}) is the solute concentration at the membrane surface. L_P stands for the hydraulic permeability of the membrane (L.h^{-1}.bar^{-1}). σ represents the reflection coefficient, a dimensionless quantity. P_s signifies the solute permeability (m.s^{-1}).

The product ($\sigma.\Delta \Pi$) as the initial pressure, also referred to as the critical pressure, denoted $P_c = \sigma.\Delta \Pi$. The reflection coefficient σ serves as an indicator of the membrane's relative permeability to a specific solute: $\sigma = 1$ signifies complete exclusion of the solute, whereas $\sigma = 0$

implies the membrane lacks selectivity [38]. Integrating [eq. (5) and eq. (6)] with eq. (1) and considering the limit conditions of the problem ($C_m = C_f$ for $x = 0$, and $C_m = C_p$ for $x = \Delta x$) results in [eq. (7) and eq. (8)] [39]:

$$R = 1 - \frac{C_p}{C_f} = \frac{\sigma(1 - F)}{1 - \sigma F} \tag{7}$$

$$F = exp\left(-\frac{(1 - \sigma)J_v}{P_s}\right) \tag{8}$$

Where F is a dimensionless flow parameter, and Δx is the membrane thickness (m) [40], [41].

Measurement and Calculation of Key Parameters

Throughout the experiments, three key parameters were systematically monitored and recorded. The first parameter is the permeate flux. This crucial parameter, indicative of membrane performance, was calculated using the equation (2) [34].

The second parameter of interest is the recovery rate ($Y\%$). This metric serves as a vital indicator of process efficiency and was calculated as the ratio of permeate flow (Q_p (l.h^{-1})) to feed flow (Q_0 (l.h^{-1})), expressed as a percentage:

$$Y = \frac{Q_P}{Q_0} \cdot 100 \tag{9}$$

The third parameter of interest is the salt rejection ($R\%$). This metric is crucial for evaluating the effectiveness of the membranes in removing salt from the feed water. Salt rejection ($R\%$) was quantified using the eq. (7) as mentioned above.

Particle swarm optimization method

The PSO algorithm, inspired by the social behavior of bird flocks [42], has widespread applications in various domains, such as nonlinear function optimization [43], and for neural network training [44]. The PSO algorithm's idea came from simulating the social behaviour of flocks of birds looking for food [45], [46].

In the implementation of the PSO algorithm, each bird is considered a starting particle, representing a potential solution in the search space. These particles move across the search space at the same time [47]. A position vector and a velocity vector are required in order to represent a particular particle. the former vector depicts the problem's solution, while the latter vector establishes the location updated in the subsequent iteration [47]. According to the value of the fitness function, each particle continuously tracks the optimal position of both the individual and the entire swarm in order to determine the best solution in the PSO algorithm (Figure 1a). The *i-th* particle's updated position and velocity in the *(t + 1)-th* iteration according to the following two formulas [46]:

$$\vec{X}_i(t + 1) = \vec{X}_i(t) + \vec{V}_i(t + 1) \tag{10}$$

$$\vec{V}_{(i)}(t + 1) = w\vec{V}_i(t) + C_1 r_1\left(\overrightarrow{Pbest}_i(t) - \vec{X}_i(t)\right) \\ + C_2 r_2\left(\overrightarrow{Gbest}_i(t) - \vec{X}_i(t)\right) \tag{11}$$

Where $\vec{X}_i(t)$ and $\vec{V}_i(t)$ represent the position and velocity of the *i-th* particle in the *t-th* iteration. $\overrightarrow{Pbest}_i(t)$ and $\overrightarrow{Gbest}_i(t)$ denote the best position of the *i-th* particle and that of the entire swarm, respectively. *t* and *t + 1* are the *t-th* and the *(t + 1)-th* iteration, respectively. *r1* and *r2* signify the uniformly distributed random numbers in [0,1] at each iteration. *w* is the inertia weight controlling the search space scope, while C_1 and C_2 denote the individual and social factors influencing particle velocity [42]. The flowchart for the basic PSO algorithm is shown in Figure 1b.
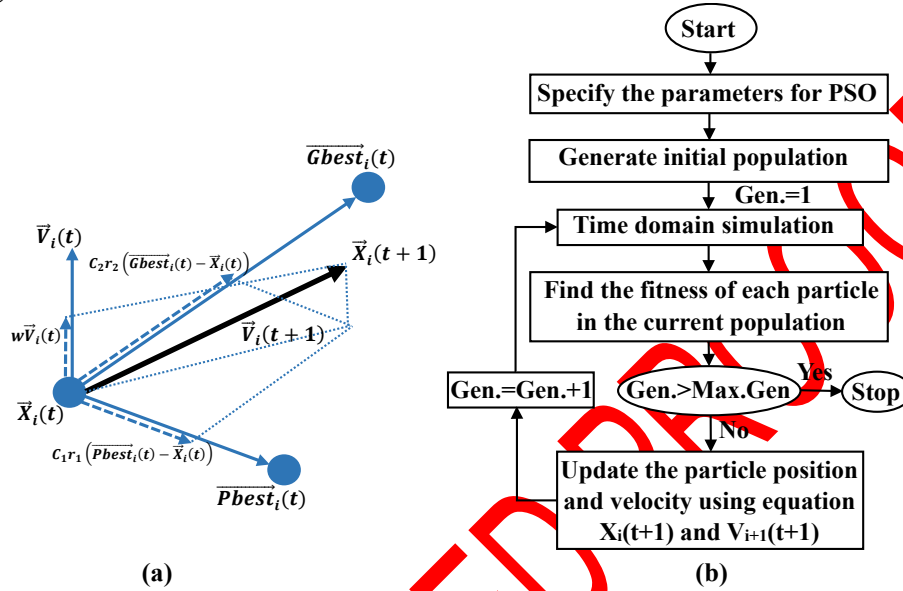

Figure 1. The motion of particles (a), and flowchart (b) of the standard PSO algorithm.

The PSO algorithm was utilized to optimize the parameters σ and Ps, crucial in membrane modelling. These parameters characterize membrane imperfections and significantly impact its performance. Leveraging PSO allows for accurate estimation of these parameters, considering concentration-dependent behaviour and enhancing the precision of membrane transport phenomena modelling. This methodological approach not only improves model accuracy but also contributes to advancements in membrane technology and process optimization.

Grey wolf optimization method

The GWO, introduced by Mirjalili in 2014 [48], is a swarm-based algorithm inspired by the hierarchical hunting behavior of grey wolves [18]. Unlike PSO, GWO is more memory-efficient, utilizing a single vector of position and retaining only the three best solutions [49]. This algorithm organizes the population of potential solutions into four hierarchical layers (Figure 2) [50]. The Alpha (α) wolf symbolizes the best solution found, leading and coordinating the search. The Beta (β) and Delta (δ) wolves represent the second-best and intermediate solutions, respectively, contributing to the balance between exploration and exploitation [51]. All other possible solutions are considered as Omega (ω) wolves, which are the least dominant and explore extensively to ensure diversity and prevent premature convergence. Through iterative position updates, GWO mimics wolf pack dynamics to efficiently converge toward the optimal solution, thereby advancing the search process [52].
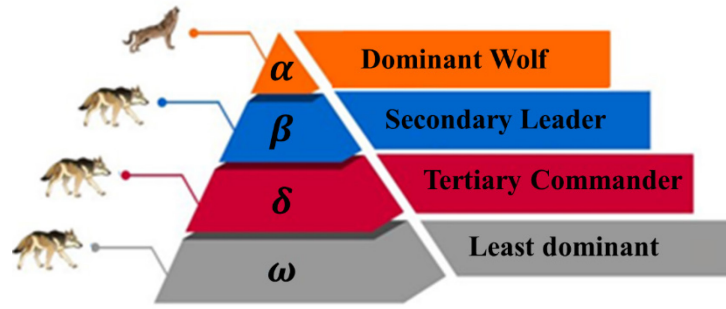
Figure 2. The social hierarchy of grey wolves, where dominance progressively decreases from the highest rank downwards

GWO is based on three key steps: encircling, hunting, and attacking prey [52]. During the encirclement phase, wolves gradually close in on their target, a strategy mirrored in GWO where search agents progressively converge towards the optimal solution (Figure 3).
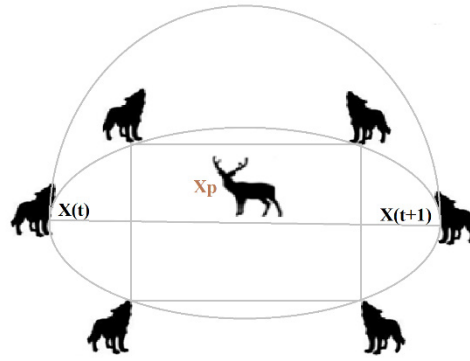

Figure 3. Illustrative representation of wolves encircling their prey

Mathematically, GWO simulates this encirclement by considering two points within an n-dimensional search space and updating the position of one point relative to the other. The mathematical model for encircling prey is given by [18]:

$$\vec{D} = \left| \vec{C} \vec{X}_p(t) - \vec{X}_w(t) \right| \tag{12}$$

$$\vec{X}_w(t + 1) = \vec{X}_p(t) - \vec{A}\,\vec{D} \tag{13}$$

Where, $X_w(t + 1)$ represents the subsequent position vector of the wolf at iteration $t+1$, while $X_w(t)$ signifies its current position vector at iteration t, and $X_p(t)$ is the position vector of the prey (best solution). The coefficient vectors $\vec{A}$ and $\vec{C}$, along with the distance vector $\vec{D}$ between the wolf and prey, influence the wolf's movement. The calculation of vectors $\vec{A}$ and $\vec{C}$ is according to [eq. (14) and eq. (15)] [18]:

$$\vec{A} = 2\vec{a}\,\vec{r}_1 - \vec{a} \tag{14}$$

$$\vec{C} = 2\,\vec{r}_2 \tag{15}$$

The variables $\vec{r}_1$ et $\vec{r}_2$ are derived from the random vectors within the range [0, 1], whereas $\vec{a}$ is a vector with identical elements. To simulate the encircling behavior, the value of its elements gradually lowered from 2 to 0 throughout iterations [52].

The hunting phase in GWO simulates the collaborative effort of wolves to locate and encircle prey. Alpha, beta, and delta wolves, representing the top three solutions, guide the

pack towards the optimal solution. These leaders, considered to have a superior understanding of the search space, direct the remaining wolves (omega) in their pursuit [51]. By following the positions of alpha, beta, and delta, the wolves gradually converge towards the potential prey position, mimicking the encirclement behaviour observed in real wolf packs.

The mathematical model of an individual grey wolf tracking the location of its prey is described as follows [52]:

$$\vec{D}_\alpha = \left| \vec{C}_1 \times \vec{X}_\alpha - \vec{X} \right| \tag{16}$$

$$\vec{D}_\beta = \left| \vec{C}_2 \times \vec{X}_\beta - \vec{X} \right| \tag{17}$$

$$\vec{D}_\delta = \left| \vec{C}_3 \times \vec{X}_\delta - \vec{X} \right| \tag{18}$$

Where $\vec{D}_\alpha$, $\vec{D}_\beta$, and $\vec{D}_\delta$ denote the distances between α, β and δ and other individuals, respectively; $\vec{X}_\alpha$, $\vec{X}_\beta$, and $\vec{X}_\delta$ denote the current positions of α, β and δ, respectively; $\vec{C}_1$, $\vec{C}_2$ and $\vec{C}_3$ are random vectors, $\vec{X}$ is the current location of the grey wolf. These equations simulate the search process [52].

$$\vec{X}_1 = \vec{X}_\alpha(t) - \vec{A}_1 \times \vec{D}_\alpha \tag{19}$$

$$\vec{X}_2 = \vec{X}_\beta(t) - \vec{A}_1 \times \vec{D}_\beta \tag{20}$$

$$\vec{X}_3 = \vec{X}_\delta(t) - \vec{A}_1 \times \vec{D}_\delta \tag{21}$$

Where $\vec{X}_1$, $\vec{X}_2$ and $\vec{X}_3$ are the positions of alpha, beta and delta wolves, respectively; $\vec{A}_1$, $\vec{A}_2$ and $\vec{A}_3$ are random vectors satisfying the restrictions of eq. (14). {[eq. (19), eq. (20) and eq. (21)]} defines the step length and direction of ω individuals in the wolf pack toward α, β and δ, respectively, and eq. (22) defines the update position of ω [52].

$$\vec{X}(t+1) = \frac{1}{3}\vec{X}_1 + \frac{1}{3}\vec{X}_2 + \frac{1}{3}\vec{X}_3 \tag{22}$$

In GWO algorithm, the new solution is randomly positioned within the regions defined by alpha, beta and delta, and updated based on these three best solutions, as shown in Figure 4a. Compared to other metaheuristics algorithms, GWO stands out due to its simplicity, efficiency, and ability to maintain a suitable equilibrium between diversification and intensification, making it applied in various engineering domains [51]. The flowchart for the basic GWO algorithm is shown in Figure 4b.

The GWO algorithm was employed to fine-tune the parameters σ and Ps, which are pivotal in membrane modelling. These parameters describe membrane imperfections and have a profound influence on its performance. By leveraging the collaborative strategies of alpha, beta, and delta wolves, GWO identifies the optimal parameter values, which enhance the accuracy of the membrane transport phenomena and contribute to significant advancements in membrane technology and process optimization.
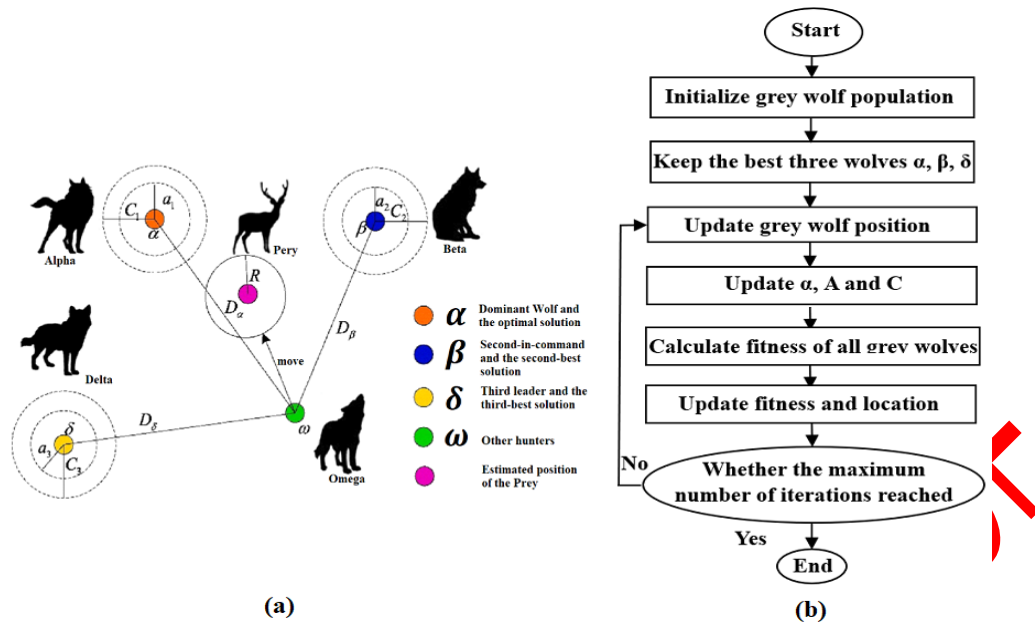
Figure 4. Position updating of the omega wolf, based on the positions of the three leading wolves (a), flowchart for the basic GWO algorithm (b)

Models Implementation and Evaluation

In this study, two advanced bio-inspired metaheuristic algorithms in conjunction with the Spiegler-Kedem Model (SKM) were implemented and evaluated to optimize salt rejection in NF and RO membranes. The two algorithms applied are PSO and GWO, each offering unique advantages for enhancing the predictive accuracy and efficiency of the SKM, are shown in Figure 5.

The implementation SKM-PSO model begins with the initialization of input data, which is processed through the Spiegler-Kedem Model to generate initial predictions. These predictions undergo an error evaluation phase, providing necessary feedback to the PSO algorithm. The PSO algorithm initializes particles, evaluates them, updates their positions, and iteratively searches for the best solution, which optimizes the SKM parameters (σ and Ps). This optimized solution is then used to produce refined predictions.

Similarly, the SKM-GWO model, follows a parallel structure. Input data is fed into the Spiegler-Kedem Model to generate initial predictions, followed by error evaluation. The GWO algorithm then initializes a pack of wolves, evaluates them, updates their positions based on social hierarchy, and searches for the optimal solution. The best solution obtained is used to optimize the SKM parameters, resulting in improved predictive accuracy.

Both models have been rigorously evaluated to ensure robustness and precision in predicting membrane performance. The integration of PSO and GWO with the Spiegler-Kedem Model provides a comprehensive approach to membrane modelling, leveraging the strengths of metaheuristic optimization to enhance the accuracy and efficiency of salt rejection predictions.
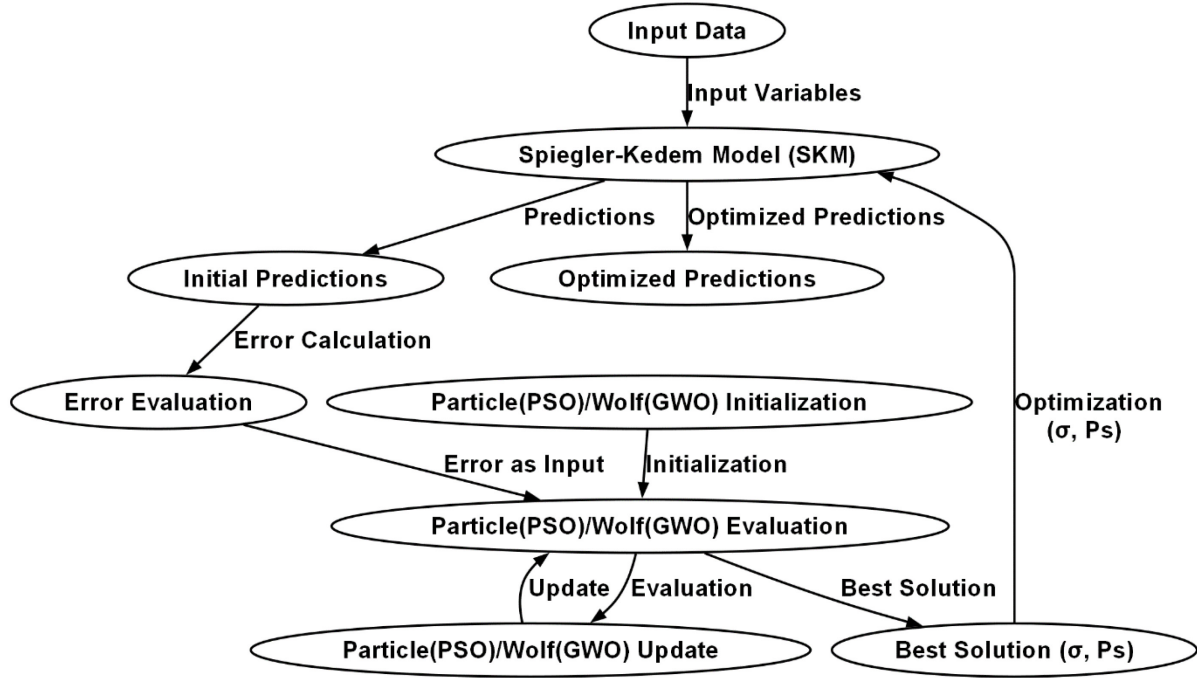
Figure 5. Implementation and optimization frameworks for SKM-PSO and SKM-GWO models

The statistical indicators used to evaluate the performance of the SKM-PSO approach are: the mean absolute error (MAE), the mean squared error (MSE), the root-mean squared error (RMSE), the normalized objective function (NOF), the Nash-Sutcliffe coefficient (NSC), and R-squared values (R^2). The equations used to determine these indicators are given by [53], [54]:

$$MAE = \frac{1}{n}\sum_{i=1}^{n}\left|R_{exp,i} - R_{pred,i}\right| \tag{23}$$

$$MSE = \frac{1}{n}\sum_{i=1}^{n}\left(R_{exp,i} - \bar{R}_{exp}\right)^2 \tag{24}$$

$$RMSE = \sqrt{\left[\frac{\sum_{i=1}^{n}\left(R_{exp,i} - R_{pred,i}\right)^2}{n}\right]} \tag{25}$$

$$NOF = \left[\frac{RMSE}{\bar{\bar{R}}_{exp}}\right] \tag{26}$$

$$NSC = 1 - \left[\frac{\sum_{i=1}^{n}\left(R_{exp,i} - R_{pred,i}\right)^2}{\sum_{i=1}^{n}\left(R_{exp,i} - \bar{R}_{pred}\right)^2}\right] \tag{27}$$

$$R^2 = 1 - \left[\frac{\sum_{i=1}^{n}\left(R_{exp,i} - R_{pred,i}\right)^2}{\sum_{i=1}^{n}\left(R_{exp,i} - \bar{R}_{exp}\right)^2}\right] \tag{28}$$

The coefficient MAE provides an indication of the average absolute error of the model, regardless of the direction of the errors. A lower MAE indicates better model performance. The MSE provides an indication of the spread of errors, giving more weight to larger errors due to squaring. A lower MSE indicates better fit between the model predictions and the actual data [29]. The RMSE provides a rating for the model error and shows a perfect similarity between the values that are observed and those predicted, in case of being equal to 0. For NOF, when it is less than 1, the model error is said to be negligible, and the NSC ranges from -∞ to 1, a value close to 1 mark that the model is well performed.

DATA, RESULTS AND DISCUSSION

This section provides an overview of the study area and the specific characteristics of the feed water and membranes used in this research. Additionally, the attributes of the NF and RO membranes employed in the experiments were detailed, along with the methodology for measuring and calculating key performance parameters.

Study area: Tan Tan city, Morocco

Tan-Tan City, situated in the arid, water scarce south of Morocco (Figure 6), is an important site for understanding the challenges of water desalination due to its proximity to brackish water sources [24]. The city experiences significant problems with water salinity, which impacts both agricultural activities and the availability of potable water for residents [26]. The primary source of water in Tan-Tan comes from the nearby Oued Draâ and coastal aquifers, which are prone to saltwater intrusion due to over-extraction and climatic conditions.
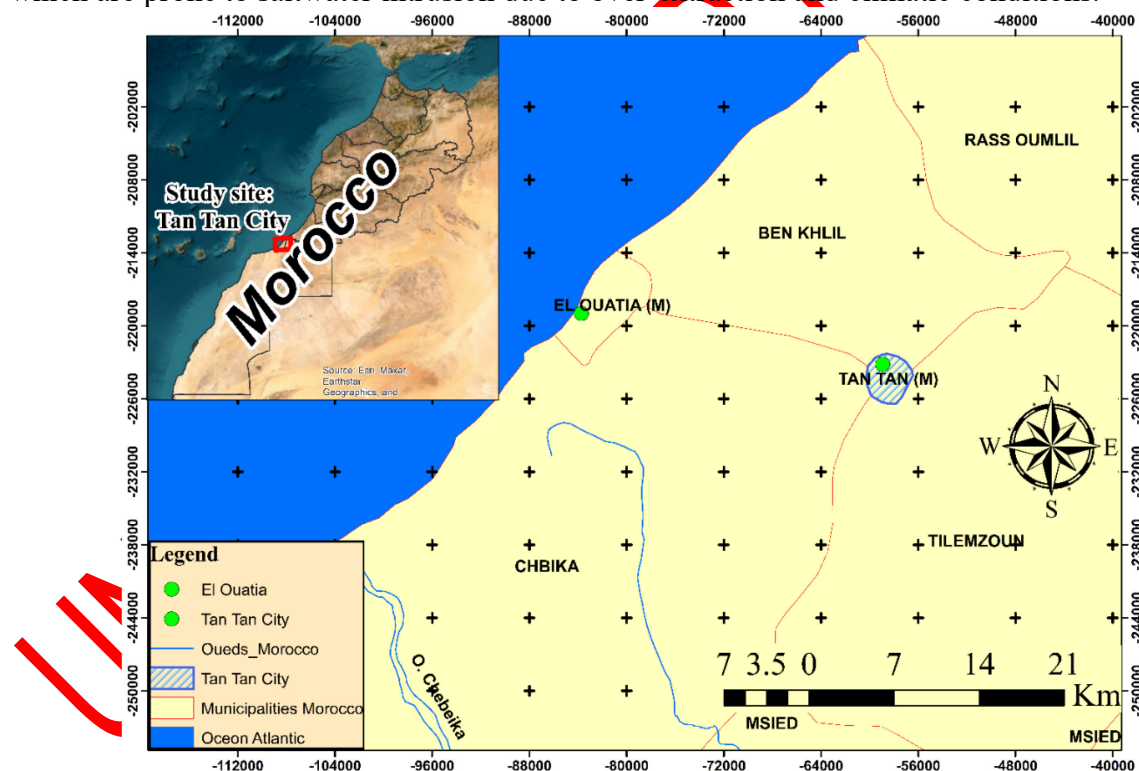

Figure 6. Study area: Tan-Tan City, Morocco

Tan-Tan is emblematic of the larger regional challenge of balancing water needs for a growing population and agricultural demands with the limitations posed by saline water sources. The arid local climate, characterized by limited rainfall, intensifies the water scarcity challenge. As a result, advanced desalination techniques, such as NF and RO, are indispensable for maintaining a sustainable water supply. In an effort to identify the most suitable and cost-effective solution, particularly concerning energy efficiency for a long-term water supply for Tan-Tan City, and to gain proficiency in new technologies [55], ONEE (Office National de

Abbi, B., Touazit, A., *et al.*
Modelling Salt Rejection in Nanofiltration and Reverse...

Year 2025
Volume 13, Issue 3, 1130565

l'Électricité et de l'Eau potable) carried out technical and economic studies on various thermal and membrane technologies. These studies also examined energy sources such as fossil fuels, solar power, gravity, and nuclear energy, while considering their long-term environmental impacts.

Tan-Tan faces significant challenges, particularly in managing the high levels of Total Dissolved Solids (TDS) in the water, which often exceed WHO safety standards for drinking water [27]. Addressing these issues necessitates the deployment of effective desalination technologies and strategies for sustainable water management. Pilot studies and research in Tan-Tan are focus to optimizing membrane technologies to lower salinity levels and ensure a consistent supply of safe drinking water.

This description provides a detailed overview of Tan-Tan City as a study site, underscoring the critical role of desalination research in addressing the dual challenges of water scarcity and salinity.

Characteristics of the feed water

The characteristics of the feed water of Tan Tan city (Table 1) can be obtained from ONEE. The pH measurement of 7.9 indicates that the water is slightly alkaline, which can impact its chemical behaviour and compatibility with certain materials. Temperature is an important parameter to monitor as it can influence various water properties and reactions. With a recorded temperature of 27.0°C, the water falls within a typical range for ambient conditions.

The concentrations of specific ions in the water, such as chloride (1287-1349) (ppm), calcium 270 (ppm), magnesium 115 (ppm), sodium (595-761) (ppm), potassium 19 (ppm), and sulphate 500 (ppm), provide insights into its chemical composition. These ions play crucial roles in various chemical reactions and processes, including membrane filtration and desalination. Table1 shows that several parameters of water quality exceed both WHO (World Health Organization) and Moroccan standards for drinking water. In specifically, TDS and ion concentrations Na+, SO42-, and Cl- are high, indicating a need for desalination.

Overall, these detailed analytical results provide valuable information about the feed water used in the experiments, enabling researchers to assess its suitability for membrane filtration studies and evaluate potential challenges or considerations during the experimental process.

Table 1. Feed water characteristics compared with Moroccan and WHO standards [26].

	Tan Tan feed water	Moroccan standards	WHO standards
T(°C)	27	-	25
pH	7.9	6.0 – 9.2	6.5 – 8.5
TDS (ppm)	3300	<1000	<1000
Cl- (ppm)	1287	<250	<250
NO3- (ppm)	20	<50	<50
F- (ppm)	1.1	1.5	0.5 - 1.5
SO42- (ppm)	500	200	250
Ca2+ (ppm)	270	<500	<270
Mg2+(ppm)	115	100	<50
Na+ (ppm)	595	<200	<200
K+ (ppm)	19	-	10

Characteristics of Nanofiltration and Reverse Osmosis Membranes

In this study, three nanofiltration membranes (NF90, NF200 and NE90) and one reverse osmosis membrane (BW30LE) were used. Table 2 outlines the key characteristics of the membranes utilized in the experimental setup. The membranes selected for this investigation vary in their Molecular Weight Cut Off (MWCO) values, which determine the size of the

particles or molecules that can pass through the membrane. Additionally, the surface area of each membrane module is provided, indicating the available area for filtration processes. Notably, most of the membranes are made of polyamide, a commonly used material known for its robustness and effectiveness in membrane filtration applications, the NF200 membrane is an exception, which is made of cross-linked poly piperazine Amide with sulfonated functional groups.

Before filtration, the membranes were immersed in ultrapure water for 24 hours at 4 °C to eliminate preservatives. Each membrane was then pressurized with pure water for 15 minutes at 4 (bar) until the permeate conductivity stabilized below 1 (µS/cm). Following each run, the membranes underwent cleaning procedures using alkaline and acidic solutions as per the manufacturer's recommendations. These cleaning protocols are necessary for maintaining membrane performance and prolonging their operational lifespan by removing fouling agents and restoring permeability. Overall, the selection and characterization of membranes are crucial steps in designing and conducting membrane filtration experiments, ensuring accurate and reliable results in salt rejection studies.

Table 2. Membranes Characteristics

Membrane	Manufacturer	polymer	MWCO (Da)	Surface (m^2)
BW30LE	Dow (Filmtec)	Polyamide	187	7.6
NF200	Dow (Filmtec)	poly piperazine Amide sulfonated	401	7.6
NE90	Saehan	Polyamide	254	7.6
NF90	Dow (Filmtec)	Polyamide	213	7.6

Salt rejection efficiency is a critical aspect of membrane filtration systems, particularly in applications such as water purification and desalination. By analyzing the effects of key operational parameters, valuable insights can be gained into membrane performance and selectivity, based on the available data collected from the literature (e.g., [24], [26] and [27]). In this section, the research results were presented and a deep analysis of the findings was conducted to explore how different operating parameters affect salt rejection efficiency. Moreover, the application results for the Spiegler-Kedem thermodynamic model are highlighted, as well as the results of the optimization by PSO and GWO algorithms.

Impact of operational parameters on salt rejection efficiency

Figure 7, presents the experimental data of the Tan-Tan water permeate flux as a function of transmembrane pressure for the four tested membranes.

The fluxes exhibited a pronounced linear increase with pressure, which is a common observation in membrane filtration processes due to the proportional relationship between driving force and flux. For the NF membranes, the permeate fluxes were significantly higher compared to the RO membrane. This difference can be attributed to the larger pore size and lower selectivity of NF membranes, allowing for higher water permeability. Among the NF membranes tested, NF90 and NE90 achieved the highest fluxes. These membranes are designed for high permeability, making them suitable for applications requiring high water throughput. On the other hand, the NF200 membrane showed the lowest flux among the NF membranes tested. This lower flux could be due to its design characteristics, such as a tighter membrane structure or different material properties, which result in reduced water permeability.
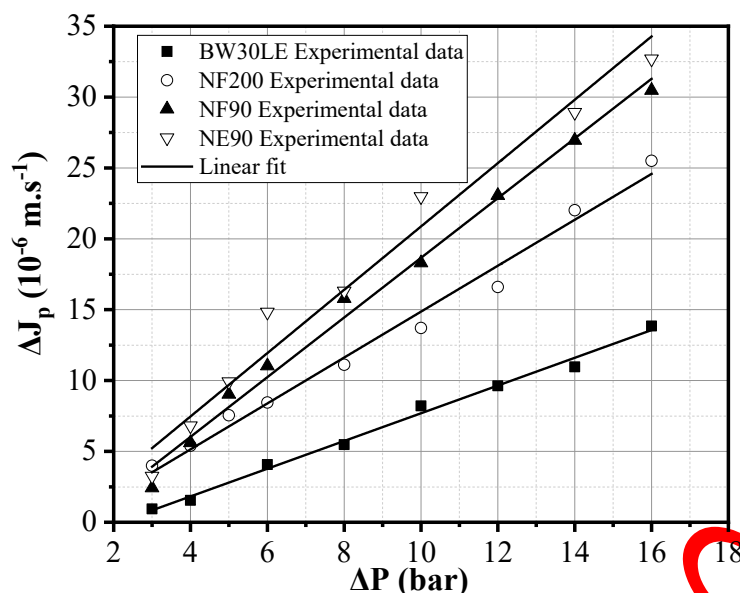
Figure 7. Effect of transmembrane pressure on the permeate flux in Tan-Tan water

The hydraulic permeability (Lp) of the saline solution was determined from the slope of the linear plot, while the x-intercept gave the critical pressure (Pc) when the transmembrane pressure equals the osmotic pressure. Table 3 provides a summary of the Lp and Pc values for all membranes tested with Tan-Tan brackish water.

The Pc of the RO membrane was approximately two to three times higher than that of the nanofiltration membrane. This difference is attributed to the higher rejection rates and the correspondingly greater osmotic pressure differential across the RO membrane. Flux was detected at pressures below 1 (bar). NF membranes offer the advantage of partial demineralization, which is linked to a lower impact of osmotic pressure on hydraulic permeability compared to RO membranes. This is expected since the concentration difference across the NF membrane is lower, resulting in reduced osmotic pressure effects. Consequently, NF membranes demonstrate higher flux rates under lower pressures compared to RO membranes.

Table 3. Hydraulic permeability (*Lp*) and critical pressures (*Pc*) to Tan-Tan water

Membranes	*Lp* (m. s⁻¹. Bar⁻¹)	*Pc* (Bar)
BW30LE	0.97	2.07
NF200	1.62	1.13
NE90	2.11	0.5
NF90	2.23	0.65

Figure 8, illustrates the evolution of total salinity rejection measurements as a function of transmembrane pressure for the four tested membranes at 15% recovery rate. This comprehensive comparison demonstrates the efficacy of each membrane under consistent operational conditions. In general, at a specific operating pressure and conversion rate, the order of total salt rejection for the membranes studied was as follows: BW30LE > NF90 > NE90 > NF200. As the pressure increases, the salt rejection improves because the higher pressure enhances the selectivity of the membrane for water over salt ions. This is due to the increased hydraulic pressure overcoming the osmotic pressure, which tends to draw salt through the membrane. Consequently, at higher pressures, more water molecules pass through the membrane while the salt ions are retained. However, at very high pressures, the marginal gains in salt rejection can diminish, highlighting the need for an optimal operating pressure to balance permeate flux and salt rejection effectively.
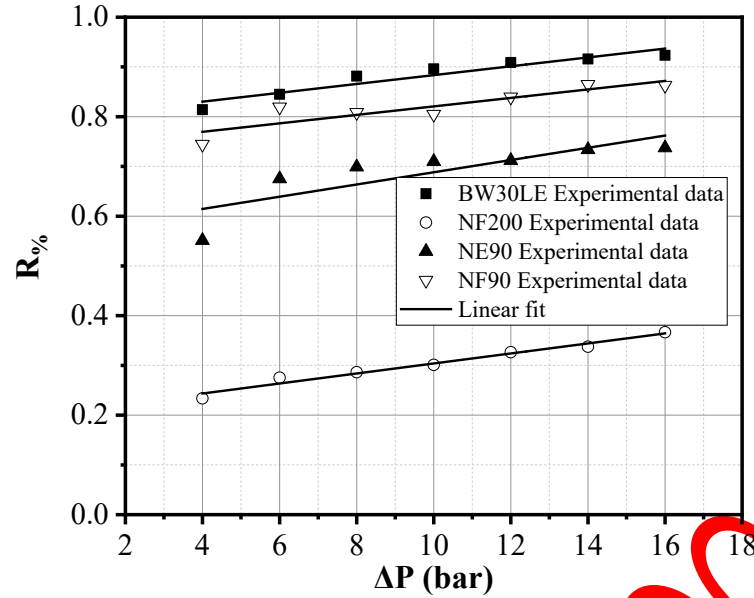
Figure 8. Total salinity rejection at 15% Recovery Rate

Model application and parameter's optimization results

The optimization process involved minimizing the objective function, which quantifies the difference between the model-predicted rejection rates and the experimental data. By iteratively adjusting the model parameters, PSO and GWO efficiently searched the parameter space to find the optimal σ and Ps values that minimized the cost function. The objective function *ObjF(x)* [56] for PSO and GWO optimization can be formulated as follows:

$$ObjF(x)_{PSO/GWO} = \sum_{i=1}^{n} \left[\left(J_i^{exp} - J_i^{pre}(\sigma, Ps) \right)^2 + \left(R_i^{exp} - R_i^{pre}(\sigma, Ps) \right)^2 \right] \tag{29}$$

Where J_i^{exp} and J_i^{pre} are the experimental and predicted water fluxes, respectively. R_i^{pre} and R_i^{pre} are the experimental and predicted salt rejections, respectively. The variable x represents the set of parameters σ and Ps that the PSO and GWO algorithms adjust to minimize the objective function.

Both optimization techniques demonstrated robust performance in calibrating the SKM parameters, enhancing the model's accuracy and reliability in predicting membrane behaviour under various operating conditions.

Figure 9 shows the predicted total salinity rejection percentages at 15% recovery rate as a function of permeate flux for four experimental membranes, using the SKM-PSO and SKM-GWO approaches and the experimental data for comparison.

The SKM-PSO and SKM-GWO predictions demonstrate the simulated rejection percentages derived from the Spiegler-Kedem Model parameters optimized using PSO and GWO algorithms. These predictions serve as theoretical representations of membrane performance, aiming to capture the underlying mechanisms governing salt rejection. Generally, a consistent trend is observed between the experimental data and the SKM-PSO, SKM-GWO approaches predictions across all membranes. This consistency indicates that the optimized Spiegler Kedem model adequately captures the salt rejection behaviour of the membranes under investigation.

As permeate flow increases, the rejection percentage tends to be asymptotic in the range of measurement. This phenomenon is expected and can be attributed to concentration polarization effects and membrane fouling, which become more pronounced at higher permeate fluxes. Noticeable differences in rejection percentages among the different membranes, both in the

experimental data and model predictions, highlight variations in membrane properties, such as pore size, surface charge, and selectivity, which influence salt rejection efficiency.

Both SKM-PSO and SKM-GWO approaches effectively capture the complex transport phenomena during membrane filtration. The agreement between the experimental data and the SKM-PSO and SKM-GWO predictions reinforces the reliability of the models in predicting salt rejection behaviour under varying operational conditions. The close alignment between the experimental data and the models demonstrates the robustness of the optimization techniques in finetuning the Spiegler-Kedem model parameters to match experimental observations.
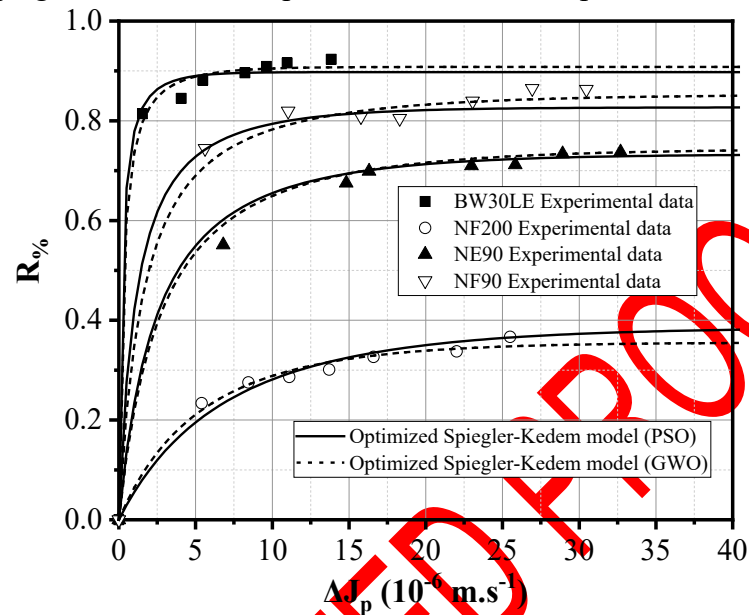

Figure 9. Experimental and predicted of Total salinity rejection at 15% recovery rate

Furthermore, the optimized parameters, including solute permeability (Ps) and the reflection coefficient (σ), obtained for 15% recovery rate for each membrane, have been compiled in Table 4. These parameters are crucial indicators of membrane performance and play a significant role in governing salt rejection efficiency under different operational conditions. On the other hand, the comparison between the SKM-PSO and SKM-GWO approaches indicates that both optimization techniques provide valuable insights into membrane performance, each excelling in different aspects such as convergence rates and accuracy. Notably, the SKM-GWO model demonstrates superior accuracy and faster convergence rates compared to the SKM-PSO model, highlighting its effectiveness in optimizing the Spiegler-Kedem model parameters for predicting salt rejection in membrane-based separation processes.

Table 4. Parameters optimized using methods (PSO and GWO)

Algorithms	PSO		GWO	
Parameters	σ	Ps ($\times 10^{-6}$)	σ	Ps ($\times 10^{-6}$)
BW30LE	0.89	0.2	0.91	0.28
NF200	0.38	6.29	0.35	4.86
NE90	0.73	2.27	0.74	2.52
NF90	0.82	1.05	0.85	1.51

The statistical calculations yield favourable results, with a low RMSE, indicating close agreement between predicted and observed values. Additionally, the NOF registers below 1, affirming the model's efficacy in fitting the data. Moreover, the NSC near 1 underscores the model's capability to closely replicate observed values. Furthermore, the MAE and MSE

complement these findings, contributing to the evidence that the approach performs effectively. For all membranes, the R^2 values obtained using the SKM-PSO algorithm are consistently lower compared to those obtained with the SKM-GWO algorithm. This indicates that the SKM-GWO approach provides more accurate predictions of salt rejection percentages (Figure 10).
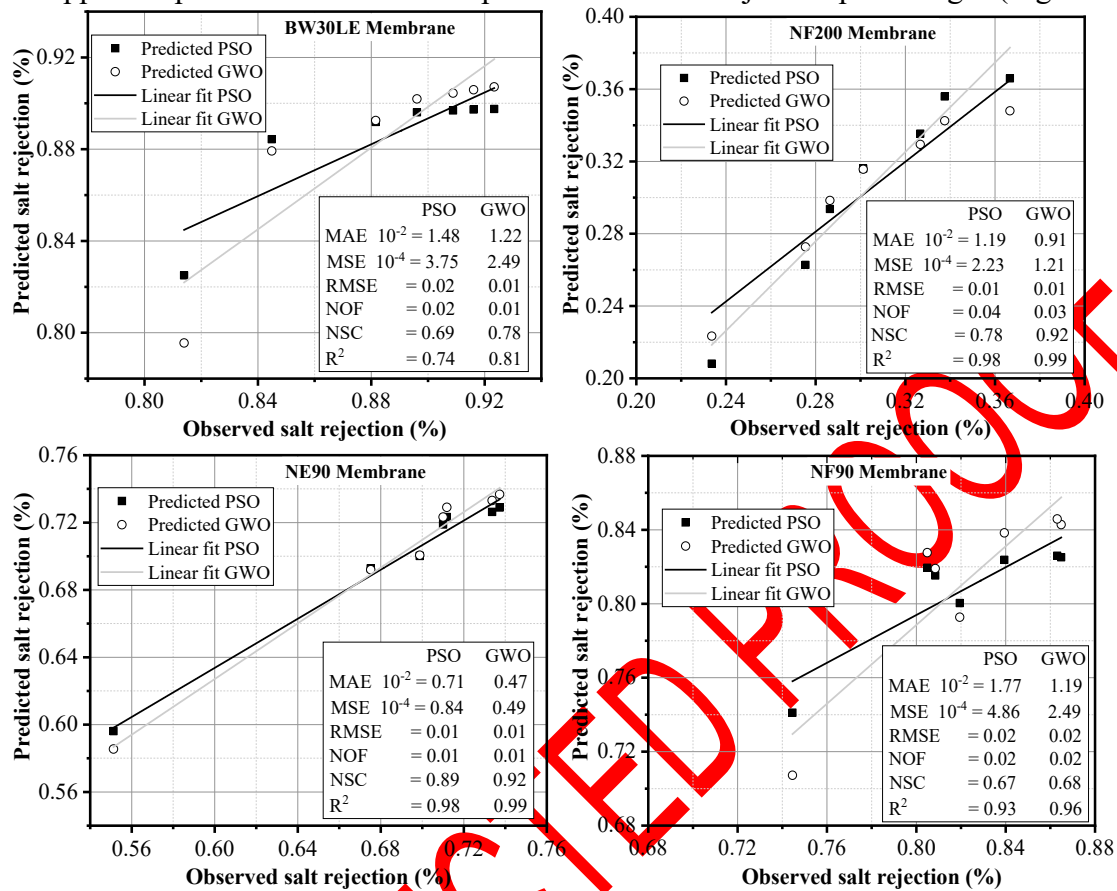

Figure 10. Parity plot comparing calculated vs. measured salt rejection with statistical criteria of parameters estimated using PSO and GWO methods for all membranes at 15% Recovery Rate.

Finally, the both models used permits a rapid assessment of salt rejection in Tan Tan City and can help to ensure the safety of water supply against excessive salinity. They calculate salt rejection adequately even at pressures where field measurements are unavailable and can be considered as a tool for support decision-making.

CONCLUSION

This study presents a comprehensive investigation into salt rejection modelling using NF and RO membranes. By integrating the Spiegler-Kedem model with PSO and GWO algorithms, a robust framework has been achieved for predicting salt rejection behaviour with enhanced accuracy and precision. Predicted results by models showed good agreement with field measurements. The model's performances were assessed using six different statistical criteria MAE, MSE, RMSE, NOF, NSC, and R² the both models were satisfactory in predicting salt rejection of the Tan-Tan city water. However, the comparison between the SKM-GWO and SKM-PSO approaches showed that the former performed better in terms of accuracy and reliability. Furthermore, experimental results indicate that NF90 membrane demonstrated higher retention capabilities, with total salinity retention between 75-90%. The developed models offer practical implications for water treatment plants, particularly in regions prone to salinity issues. They provide a valuable tool for assessing and optimizing salt rejection processes, thereby ensuring the safety and sustainability of water resources. On other hand, by continuing to innovate and refine such models, the way can be paved for more efficient and sustainable solutions to global water scarcity and pollution challenges. The model outputs

provide a foundation for future research aimed at optimizing membrane desalination processes, improving predictive accuracy in salt rejection modelling, and advancing the integration of artificial intelligence techniques, particularly machine learning, which use a minimum amount of input parameters. These models can contribute to the development of desalination strategies.

ACKNOWLEDGMENT

NOMENCLATURE

Symbols

R	Membrane rejection	(%)
Jp / Js /Jv	Permeate flux / Solute flux / Water flux	(m.s^{-1})
Cp	Solute concentration in the permeate	(mol. L^{-1})
Cf	Solute concentration in the feed solution	(mol. L^{-1})
Cm	Solute concentration within the membrane	(mol. L^{-1})
Qp	Volumetric permeate flux	(m^3. s^{-1})
S	Membrane's active area	(m^2)
Lp	Hydraulic permeability of the membrane	(m. s^{-1}. Bar^{-1})
ΔP	Transmembrane pressure	(Bar)
$\Delta\Pi$	Difference in osmotic pressure across the membrane	(Bar)
Ps	Solute permeability	(m. s^{-1})
Δx	Membrane thickness	(m)
σ	Reflection coefficient	dimensionless
Y	The recovery rate	*(%)*
$ObjF(x)$	The objective function	dimensionless
J_i^{exp} / J_i^{pre}	The experimental / predicted water flux	(m.s^{-1})
R_i^{exp}/ R_i^{pre}	The experimental / predicted salt rejection	(%)

Abbreviations

NF	Nanofiltration
RO	Reverse Osmosis
PSO	Particle Swarm Optimization
GWO	Grey Wolf Optimization
SKM	Spiegler-Kedem Model
TDS	Total Dissolved Solids
WHO	World Health Organization
ObjF	Objective Function
ONEE	National Office of Electricity and Potable Water
MWCO	Molecular Weight Cut Off

REFERENCES

[1] L. Dias Xavier, L. Yokoyama, V. Reich De Oliveira, G. Travagini Ribeiro, et O. Araujo, « The Role of Coagulation-flocculation in the Pretreatment of Reverse Osmosis in Power Plant », *J. sustain. dev. energy water environ. syst.*, vol. 8, nº 1, p. 118-131, mars 2020, doi: 10.13044/j.sdewes.d7.0266.

[2] M. Moser, F. Trieb, et T. Fichter, « Potential of Concentrating Solar Power Plants for the Combined Production of Water and Electricity in MENA Countries », *J. sustain. dev.*

energy water environ. syst., vol. 1, nº 2, p. 122-140, juin 2013, doi: 10.13044/j.sdewes.2013.01.0009.

[3] K. Zhang, H.-H. Wu, H.-Q. Huo, Y.-L. Ji, Y. Zhou, et C.-J. Gao, « Recent advances in nanofiltration, reverse osmosis membranes and their applications in biomedical separation field », *Chinese Journal of Chemical Engineering*, vol. 49, p. 76-99, sept. 2022, doi: 10.1016/j.cjche.2022.06.017.

[4] S. Honarparvar, X. Zhang, T. Chen, A. Alborzi, K. Afroz, et D. Reible, « Frontiers of Membrane Desalination Processes for Brackish Water Treatment: A Review », *Membranes*, vol. 11, nº 4, p. 246, mars 2021, doi: 10.3390/membranes11040246.

[5] H. M. Kabbani, M. Al-Hindi, G. M. Ayoub, et M. N. Ahmad, « The Effects of Salt Concentration on the Rejection of Pharmaceutically Active Compounds by Nanofiltration Membranes », *J. sustain. dev. energy water environ. syst.*, vol. 9, nº 3, p. 1-16, sept. 2021, doi: 10.13044/j.sdewes.d8.0356.

[6] X.-M. Me, Q.-L. Xie, H.-P. Xia, et W.-G. Lan, « Application of nanofiltration process in 5′-GMP production », *Desalination*, vol. 225, nº 1-3, p. 322-328, mai 2008, doi: 10.1016/j.desal.2007.07.013.

[7] A. I. Schäfer, N. Andritsos, A. J. Karabelas, E. M. V. Hoek, R. Schneider, et M. Nyström, « Fouling in Nanofiltration », in *Nanofiltration*, 1ʳᵉ éd., A. I. Schäefer et A. G. Fane, Éd., Wiley, 2021, p. 273-379. doi: 10.1002/9783527824984.ch7.

[8] R. Aridi, M. Al Mawla, E. Harika, T. Lemenand, M. Khaled, et M. Gad El-Rab, « A New Algorithmic Method for Reverse Osmosis Desalination Analysis: Design Optimization and Parametric Study », *Eng*, vol. 5, nº 3, p. 1183-1208, juin 2024, doi: 10.3390/eng5030065.

[9] P. Eriksson, « Nanofiltration extends the range of membrane filtration », *Environ. Prog.*, vol. 7, nº 1, p. 58-62, févr. 1988, doi: 10.1002/ep.3300070116.

[10] I. Sutzkover, D. Hasson, et R. Semiat, « Simple technique for measuring the concentration polarization level in a reverse osmosis system », *Desalination*, vol. 131, nº 1-3, p. 117-127, déc. 2000, doi: 10.1016/S0011-9164(00)90012-2.

[11] M. Pontié, H. Dach, J. Leparc, M. Hafsi, et A. Lhassani, « Novel approach combining physico-chemical characterizations and mass transfer modelling of nanofiltration and low pressure reverse osmosis membranes for brackish water desalination intensification », *Desalination*, vol. 221, nº 1-3, p. 174-191, mars 2008, doi: 10.1016/j.desal.2007.01.075.

[12] S. Jain et S. K. Gupta, « Analysis of modified surface force pore flow model with concentration polarization and comparison with Spiegler–Kedem model in reverse osmosis systems », *Journal of Membrane Science*, vol. 232, nº 1-2, p. 45-62, mars 2004, doi: 10.1016/j.memsci.2003.11.021.

[13] D. Van Gauwbergen et J. Baeyens, « Modelling reverse osmosis by irreversible thermodynamics », *Separation and Purification Technology*, vol. 13, nº 2, p. 117-128, avr. 1998, doi: 10.1016/S1383-5866(97)00065-8.

[14] K. S. Spiegler et O. Kedem, « Thermodynamics of hyperfiltration (reverse osmosis): criteria for efficient membranes », *Desalination*, vol. 1, nº 4, p. 311-326, déc. 1966, doi: 10.1016/S0011-9164(00)80018-1.

[15] W. R. Bowen et H. Mukhtar, « Characterisation and prediction of separation performance of nanofiltration membranes », *Journal of Membrane Science*, vol. 112, nº 2, p. 263-274, avr. 1996, doi: 10.1016/0376-7388(95)00302-9.

[16] R. Mahadeva, G. Manik, O. P. Verma, A. Goel, et S. Kumar, « Modelling and Simulation of Reverse Osmosis System Using PSO-ANN Prediction Technique », in *Soft Computing: Theories and Applications*, vol. 1053, M. Pant, T. K. Sharma, O. P. Verma, R. Singla, et A. Sikander, Éd., in Advances in Intelligent Systems and Computing, vol. 1053. , Singapore: Springer Singapore, 2020, p. 1209-1219. doi: 10.1007/978-981-15-0751-9_111.

[17] R. Mahadeva, M. Kumar, G. Manik, et S. P. Patole, « Modeling, simulation, and optimization of the membrane performance of sea-water reverse osmosis desalination plant using neural network and fuzzy based soft computing techniques », *Desalination and Water Treatment*, vol. 229, p. 17-30, juill. 2021, doi: 10.5004/dwt.2021.27386.

[18] G. R. Vakili-Nezhaad, H. Ziaiefar, S. B. Mishra, et H. Mousa, « An Optimization based Solution for Extended Spiegler-Kedem Model using Grey Wolf Optimizer », *International Journal of Engineering Research*, vol. 9, nº 02.

[19] J. Jawad, A. H. Hawari, et S. Javaid Zaidi, « Artificial neural network modeling of wastewater treatment and desalination using membrane processes: A review », *Chemical Engineering Journal*, vol. 419, p. 129540, sept. 2021, doi: 10.1016/j.cej.2021.129540.

[20] A. Maftouh *et al.*, « Solar Desalination: Current Applications and Future Potential in MENA Region – A Case Study », *J. sustain. dev. energy water environ. syst.*, vol. 11, nº 2, p. 1-26, juin 2023, doi: 10.13044/j.sdewes.d10.0437.

[21] F. Rabah, A. Mushtaha, et W. Alaloul, « Developing a framework for sustainability assessment of Reverse Osmosis desalination plants in Gaza Strip », *J. sustain. dev. energy water environ. syst.*, vol. 12, nº 1, p. 1-17, mars 2024, doi: 10.13044/j.sdewes.d11.0475.

[22] R. Rinawati *et al.*, « Enhancing Ciprofloxacin Removal: Unveiling the Potential of Graphene Oxide Synthesized from Cassava Peels through Box-Behnken Design Optimization », *J. sustain. dev. energy water environ. syst.*, vol. 12, nº 4, p. 1-20, déc. 2024, doi: 10.13044/j.sdewes.d12.0516.

[23] K. Z. Dadjiogou, A. S. A. Ajavon, et Y. Bokovi, « Energy Flow Management in a Smart Microgrid Based on Photovoltaic Energy Supplying Multiple Loads », *J. sustain. dev. energy water environ. syst.*, vol. 12, nº 1, p. 1-27, mars 2024, doi: 10.13044/j.sdewes.d11.0473.

[24] K. Tahri, « The prospects of fresh water supply for Tan City from non-conventional water resources », *Desalination*, vol. 135, nº 1, p. 43-50, 2001, doi: https://doi.org/10.1016/S0011-9164(01)00137-0.

[25] M. Pontié *et al.*, « Chapter 2 Water Defluoridation Processes: A Review. Application: Nanofiltration (NF) for Future Large-Scale Pilot Plants », in *Advances in Fluorine Science*, vol. 2, Elsevier, 2006, p. 49-80, doi: 10.1016/S1872-0358(06)02002-1.

[26] H. Dach, « Comparaison des opérations de nanofiltration et d'osmose inverse pour le dessalement sélectif des eaux saumâtres : de l'échelle du laboratoire au pilote industriel », These de doctorat, Angers, 2008. Consulté le: 17 février 2025. [En ligne]. Disponible sur: https://theses.fr/2008ANGE0032

[27] M. Pontie, H. Dach, A. Lhassani, et C. K. Diawara, « Water defluoridation using nanofiltration vs. reverse osmosis: the first world unit, Thiadiaye (Senegal) », *Desalination and Water Treatment*, vol. 51, nº 1-3, p. 164-168, janv. 2013, doi: 10.1080/19443994.2012.704715.

[28] A. Lhassani, H. Dach, et Y. A. Boussouga, « Brackish water desalination using nanofiltration membranes in Morocco », *Desalination and Water Treatment*, vol. 83, p. 288-293, juill. 2017, doi: 10.5004/dwt.2017.21221.

[29] A. Touazit, Y. Nizar, I. Nizar, F. Lahlou, et M. Igouzal, « Prediction of water temperature of Sebou estuary (Morocco) using ANN and LR », *Journal of Applied Water Engineering and Research*, vol. 12, nº 3, p. 287-296, juill. 2024, doi: 10.1080/23249676.2024.2303150.

[30] N. Zouhri, M. Igouzal, M. Larif, M. Hafsi, M. Taky, et A. Elmidaoui, « Prediction of salt rejection by nanofiltration and reverse osmosis membranes using Spiegler-Kedem model and an optimisation procedure », *Desalination and Water Treatment*, vol. 120, p. 41-50, juill. 2018, doi: 10.5004/dwt.2018.21410.

[31] M. Igouzal, F. El Azhar, M. Hafsi, M. Taky, et A. Elmidaoui, « Removal of hardness from groundwater using two nanofiltration membranes: experimental study and modeling »,

Abbi, B., Touazit, A., *et al.*
Modelling Salt Rejection in Nanofiltration and Reverse...

Year 2025
Volume 13, Issue 3, 1130565

Desalination and Water Treatment, vol. 93, p. 30-39, oct. 2017, doi: 10.5004/dwt.2017.20980.

[32] V. L. Golovashin, S. I. Lazarev, et V. V. Mamontov, « Kinetic Characteristics of Reverse-Osmosis Separation of an Aqueous Solution of Aniline in a Flat-Frame Apparatus », *Russ J Appl Chem*, vol. 78, nº 7, p. 1096-1100, juill. 2005, doi: 10.1007/s11167-005-0457-y.

[33] K. Košutić et B. Kunst, « Removal of organics from aqueous solutions by commercial RO and NF membranes of characterized porosities », *Desalination*, vol. 142, nº 1, p. 47-56, janv. 2002, doi: 10.1016/S0011-9164(01)00424-6.

[34] J. Kheriji, D. Tabassi, I. Bejaoui, et B. Hamrouni, « Boron removal from model water by RO and NF membranes characterized using S-K model », *Membrane and Water Treatment*, vol. 7, nº 3, p. 193-207, 2016, doi: 10.12989/MWT.2016.7.3.193.

[35] R. R. Nair, E. Protasova, S. Strand, et T. Bilstad, « Implementation of Spiegler–Kedem and Steric Hindrance Pore Models for Analyzing Nanofiltration Membrane Performance for Smart Water Production », *Membranes*, vol. 8, nº 3, p. 78, sept. 2018, doi: 10.3390/membranes8030078.

[36] O. Kedem et A. Katchalsky, « Permeability of composite membranes. Part 1.—Electric current, volume flow and flow of solute through membranes », *Trans. Faraday Soc.*, vol. 59, nº 0, p. 1918-1930, 1963, doi: 10.1039/TF9635901918.

[37] Z. V. P. Murthy et S. K. Gupta, « Estimation of mass transfer coefficient using a combined nonlinear membrane transport and film theory model », *Desalination*, vol. 109, nº 1, p. 39-49, mars 1997, doi: 10.1016/S0011-9164(97)00051-9.

[38] J. Schaep, B. Van Der Bruggen, C. Vandecasteele, et D. Wilms, « Influence of ion size and charge in nanofiltration », *Separation and Purification Technology*, vol. 14, nº 1-3, p. 155-162, août 1998, doi: 10.1016/S1383-5866(98)00070-7.

[39] N. Hilal, H. Al-Zoubi, A. W. Mohammad, et N. A. Darwish, « Nanofiltration of highly concentrated salt solutions up to seawater salinity », *Desalination*, vol. 184, nº 1-3, p. 315-326, nov. 2005, doi: 10.1016/j.desal.2005.02.062.

[40] M. D. Murcia, M. Gomez, E. Gomez, A. Bodalo, J. L. Gomez, et A. M. Hidalgo, « Assessing combination treatment, enzymatic oxidation and ultrafiltration in a membrane bioreactor, for 4-chlorophenol removal: Experimental and modeling », *Journal of Membrane Science*, vol. 342, nº 1-2, p. 198-207, oct. 2009, doi: 10.1016/j.memsci.2009.06.037.

[41] A. M. Hidalgo, G. León, M. Gómez, M. D. Murcia, E. Gómez, et J. L. Gómez, « Application of the Spiegler–Kedem–Kachalsky model to the removal of 4-chlorophenol by different nanofiltration membranes », *Desalination*, vol. 315, p. 70-75, avr. 2013, doi: 10.1016/j.desal.2012.10.008.

[42] J. Kennedy et R. C. Eberhart, « A discrete binary version of the particle swarm algorithm », in *Computational Cybernetics and Simulation 1997 IEEE International Conference on Systems, Man, and Cybernetics*, oct. 1997, p. 4104-4108 vol.5. doi: 10.1109/ICSMC.1997.637339.

[43] G. H. Li, Z. L. Sun, et S. X. Hu, « Prediction of Salinity in Qiantang Estuary Based on Wavelet Neural Network Optimized by Particle Swarm Optimization », *AMM*, vol. 353-356, p. 2683-2687, août 2013, doi: 10.4028/www.scientific.net/AMM.353-356.2683.

[44] X. Lin et Y. Li, « Ocean salinity intelligent prediction model based on particle swarm optimization LSTM neural network », in *2022 3rd Asia-Pacific Conference on Image Processing, Electronics and Computers*, Dalian China: ACM, avr. 2022, p. 652-657. doi: 10.1145/3544109.3544328.

[45] Eberhart et Yuhui Shi, « Particle swarm optimization: developments, applications and resources », in *Proceedings of the 2001 Congress on Evolutionary Computation (IEEE Cat. No.01TH8546)*, Seoul, South Korea: IEEE, 2001, p. 81-86. doi: 10.1109/CEC.2001.934374.

[46] F. Marini et B. Walczak, « Particle swarm optimization (PSO). A tutorial », *Chemometrics and Intelligent Laboratory Systems*, vol. 149, p. 153-165, déc. 2015, doi: 10.1016/j.chemolab.2015.08.020.

[47] Y. Han, J. Luo, et X. Xu, « On the Constellation Design of Multi-GNSS Reflectometry Mission Using the Particle Swarm Optimization Algorithm », *Atmosphere*, vol. 10, nº 12, p. 807, déc. 2019, doi: 10.3390/atmos10120807.

[48] S. Mirjalili, S. M. Mirjalili, et A. Lewis, « Grey Wolf Optimizer », *Advances in Engineering Software*, vol. 69, p. 46-61, mars 2014, doi: 10.1016/j.advengsoft.2013.12.007.

[49] M. H. Nadimi-Shahraki, S. Taghian, et S. Mirjalili, « An improved grey wolf optimizer for solving engineering problems », *Expert Systems with Applications*, vol. 166, p. 113917, mars 2021, doi: 10.1016/j.eswa.2020.113917.

[50] S. M. Ebrahimi, S. Hasanzadeh, et S. Khatibi, « Parameter identification of fuel cell using Repairable Grey Wolf Optimization algorithm », *Applied Soft Computing*, vol. 147, p. 110791, nov. 2023, doi: 10.1016/j.asoc.2023.110791.

[51] O. Gliti, M. Chafik El Idrissi, et M. Igouzal, « Intelligent Design of an Ultra-Thin Near-Ideal Multilayer Solar Selective Absorber Using Grey Wolf Optimization linked to Deep Learning », *Ecol. Eng. Environ. Technol.*, vol. 25, nº 2, p. 70-87, févr. 2024, doi: 10.12912/27197050/175785.

[52] K. Zhou, C. Tan, Y. Zhao, J. Yu, Z. Zhang, et Y. Wu, « Research on Solving Flexible Job Shop Scheduling Problem Based on Improved GWO Algorithm SS-GWO », *Neural Process Lett*, vol. 56, nº 1, p. 26, févr. 2024, doi: 10.1007/s11063-024-11488-1.

[53] M. Bchiti, M. Igouzal, S. El-Ghzizel, et A. E. Midaoui, « Modeling pore blocking of nanofiltration and reverse osmosis membranes during NaCl removal ».

[54] M. Bchiti, M. Igouzal, F. E. Azhar, H. Oudda, et A. E. Midaoui, « Modeling the separation performance of nanofiltration and reverse osmosis: case study of groundwater desalination (M'Nasra zone Morocco) ».

[55] Z. Wenxiang, Z. Yajun, Z. Dafang, et D. Duo, « Pre-project study of a nuclear desalination demonstration plant for Tan-Tan, Morocco », *Nuclear Engineering and Design*, vol. 213, nº 2-3, p. 279-287, avr. 2002, doi: 10.1016/S0029-5493(01)00520-9.

[56] J. Liu, H. Ma, X. Ren, T. Shi, P. Li, et X. Ma, « The continuous-discrete PSO algorithm for shape formation problem of multiple agents in two and three dimensional space », *Applied Soft Computing*, vol. 67, p. 409-433, juin 2018, doi: 10.1016/j.asoc.2018.02.015.